

In-flight observations of low-mode pR asymmetries in NIF implosions^{a)}

A. B. Zylstra, J. A. Frenje, F. H. Séguin, J. R. Rygg, A. Kritcher, M. J. Rosenberg, H. G. Rinderknecht, D. G. Hicks, S. Friedrich, R. Bionta, N. B. Meezan, R. Olson, J. Atherton, M. Barrios, P. Bell, R. Benedetti, L. Berzak Hopkins, R. Betti, D. Bradley, D. Callahan, D. Casey, G. Collins, E. L. Dewald, S. Dixit, T. Döppner, M. J. Edwards, M. Gatū Johnson, S. Glenn, G. Grim, S. Hatchett, O. Jones, S. Khan, J. Kilkenny, J. Kline, J. Knauer, G. Kyrala, O. Landen, S. LePape, C. K. Li, J. Lindl, T. Ma, A. Mackinnon, M. J.-E. Manuel, D. Meyerhofer, E. Moses, S. R. Nagel, A. Nikroo, T. Parham, A. Pak, R. D. Petrasso, R. Prasad, J. Ralph, H. F. Robey, J. S. Ross, T. C. Sangster, S. Sepke, N. Sinenian, H. W. Sio, B. Spears, R. Tommasini, R. Town, S. Weber, D. Wilson, C. Yeamans, and R. Zacharias

Citation: *Physics of Plasmas* (1994-present) **22**, 056301 (2015); doi: 10.1063/1.4918355

View online: <http://dx.doi.org/10.1063/1.4918355>

View Table of Contents: <http://scitation.aip.org/content/aip/journal/pop/22/5?ver=pdfcov>

Published by the [AIP Publishing](#)

Articles you may be interested in

[Dynamic symmetry of indirectly driven inertial confinement fusion capsules on the National Ignition Facility^{a\)}](#)
Phys. Plasmas **21**, 056313 (2014); 10.1063/1.4876609

[Radiative shocks produced from spherical cryogenic implosions at the National Ignition Facility^{a\)}](#)
Phys. Plasmas **20**, 056315 (2013); 10.1063/1.4805081

[Spherical shock-ignition experiments with the 40 + 20-beam configuration on OMEGA](#)
Phys. Plasmas **19**, 102706 (2012); 10.1063/1.4763556

[Cryogenic thermonuclear fuel implosions on the National Ignition Facility^{a\)}](#)
Phys. Plasmas **19**, 056318 (2012); 10.1063/1.4719686

[Analytic criteria for shock ignition of fusion reactions in a central hot spot](#)
Phys. Plasmas **18**, 102702 (2011); 10.1063/1.3646743



In-flight observations of low-mode ρR asymmetries in NIF implosions^{a)}

A. B. Zylstra,^{1,b),c)} J. A. Frenje,¹ F. H. Séguin,¹ J. R. Rygg,² A. Kritchler,² M. J. Rosenberg,¹ H. G. Rinderknecht,¹ D. G. Hicks,^{2,d)} S. Friedrich,² R. Bionta,² N. B. Meezan,² R. Olson,^{3,4} J. Atherton,² M. Barrios,² P. Bell,² R. Benedetti,² L. Berzak Hopkins,² R. Betti,⁵ D. Bradley,² D. Callahan,² D. Casey,² G. Collins,² E. L. Dewald,² S. Dixit,² T. Döppner,² M. J. Edwards,² M. Gatu Johnson,¹ S. Glenn,² G. Grim,⁴ S. Hatchett,² O. Jones,² S. Khan,² J. Kilkenny,⁶ J. Kline,⁴ J. Knauer,⁵ G. Kyrala,⁴ O. Landen,² S. LePape,² C. K. Li,¹ J. Lindl,² T. Ma,² A. Mackinnon,² M. J.-E. Manuel,¹ D. Meyerhofer,⁵ E. Moses,² S. R. Nagel,² A. Nikroo,⁶ T. Parham,² A. Pak,² R. D. Petrasso,¹ R. Prasad,² J. Ralph,² H. F. Robey,² J. S. Ross,² T. C. Sangster,⁵ S. Sepke,² N. Sinenian,¹ H. W. Sio,¹ B. Spears,² R. Tommasini,² R. Town,² S. Weber,² D. Wilson,⁴ C. Yeamans,² and R. Zacharias²

¹Plasma Science and Fusion Center, Massachusetts Institute of Technology, Cambridge, Massachusetts 02139, USA

²Lawrence Livermore National Laboratory, Livermore, California 94550, USA

³Sandia National Laboratory, Albuquerque, New Mexico 87185, USA

⁴Los Alamos National Laboratory, Los Alamos, New Mexico 87545, USA

⁵Laboratory for Laser Energetics, University of Rochester, Rochester, New York 14623, USA

⁶General Atomics, San Diego, California 92186, USA

(Received 14 November 2014; accepted 30 January 2015; published online 15 April 2015)

Charged-particle spectroscopy is used to assess implosion symmetry in ignition-scale indirect-drive implosions for the first time. Surrogate D³He gas-filled implosions at the National Ignition Facility produce energetic protons via D+³He fusion that are used to measure the implosion areal density (ρR) at the shock-bang time. By using protons produced several hundred ps before the main compression bang, the implosion is diagnosed in-flight at a convergence ratio of 3–5 just prior to peak velocity. This isolates acceleration-phase asymmetry growth. For many surrogate implosions, proton spectrometers placed at the north pole and equator reveal significant asymmetries with amplitudes routinely $\gtrsim 10\%$, which are interpreted as $\ell = 2$ Legendre modes. With significant expected growth by stagnation, it is likely that these asymmetries would degrade the final implosion performance. X-ray self-emission images at stagnation show asymmetries that are positively correlated with the observed in-flight asymmetries and comparable in magnitude, contradicting growth models; this suggests that the hot-spot shape does not reflect the stagnated shell shape or that significant residual kinetic energy exists at stagnation. More prolate implosions are observed when the laser drive is sustained (“no-coast”), implying a significant time-dependent asymmetry in peak drive. © 2015 AIP Publishing LLC. [http://dx.doi.org/10.1063/1.4918355]

I. INTRODUCTION

The central challenge of Inertial Confinement Fusion (ICF) is to compress and heat fusion fuel to the extreme conditions required for ignition and burn.^{1,2} At the National Ignition Facility (NIF),³ the approach to achieving this is by symmetric, ablatively driven spherical compression, where the goal is a convergence ratio $CR \equiv R_{initial}/R_{final} \sim 35$.⁴ Ignition experiments must control the cold-fuel symmetry to better than several percent at stagnation.^{2,5,6} In indirect-drive implosions conducted at the NIF, radiation drive non-uniformities can cause detrimental low-mode ($\lesssim 8$) asymmetries^{7,8} the focus of this work.

Several techniques are used to study asymmetry at the NIF; in this paper, we present the first charged-particle measurements of areal-density (ρR) asymmetries at the shock-bang time in ignition-scale implosions. These measurements are

novel in quantifying ρR asymmetries that are present when the implosion is in-flight, at $CR \sim 3 - 5$, complementing prior methods at different CR . It is comparable to recently developed in-flight radiography of the imploding shell,⁹ which can be used simultaneously with the charged-particle diagnostics. Other techniques for diagnosing symmetry include “re-emit” experiments that measure x-ray re-emission from a high-Z capsule to diagnose early-time ($CR \sim 1$) hohlraum drive asymmetries^{10,11} and shock-timing experiments that use multiple views to diagnose early-time shock symmetry.^{12,13} In addition, x-ray self-emission produced by the implosion at stagnation is imaged to diagnose the final hot-spot symmetry in lower-convergence ($CR \sim 15 - 20$) surrogate implosions.¹⁴ In cryogenic implosions, the final stagnated hot-spot and cold-fuel shapes are diagnosed by x-ray¹⁵ and neutron¹⁶ imaging techniques.

This paper is organized as follows. The technique and its application to asymmetry measurements are discussed in Sec. II, the data are compared to stagnation x-ray self-emission asymmetries in Sec. III, an observed trend with coasting time is discussed in Sec. IV, and the paper is concluded in Sec. V.

^{a)}Paper No. PI1 6, Bull. Am. Phys. Soc. **59**, 237 (2014).

^{b)}Invited speaker.

^{c)}Electronic mail: zylstra@mit.edu

^{d)}Present address: Centre for Micro-Photonics, Swinburne University of Technology, Hawthorn, VIC 3122, Australia.

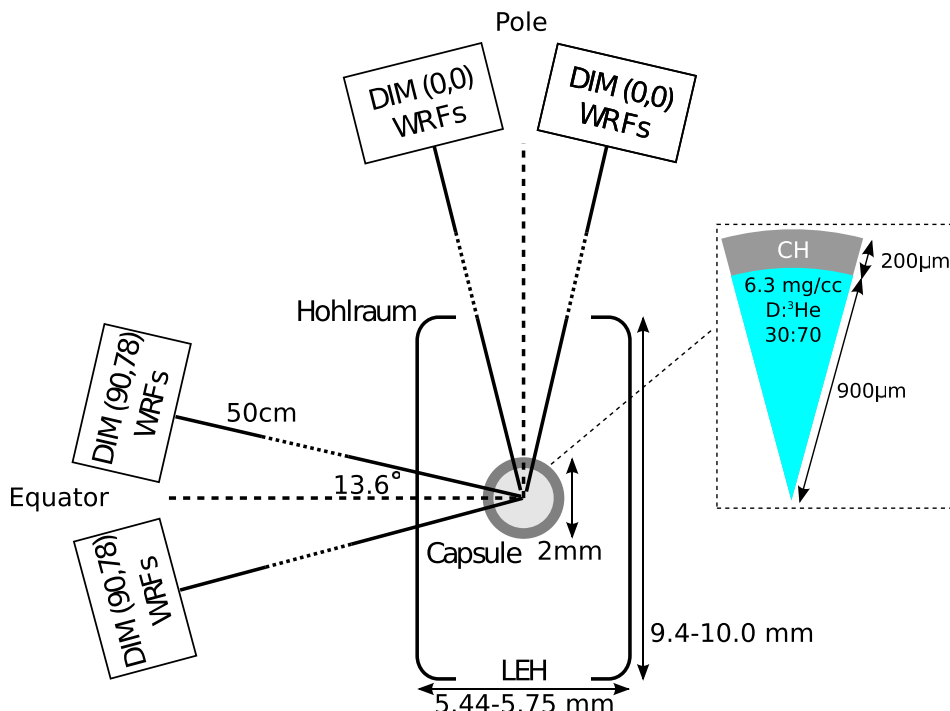
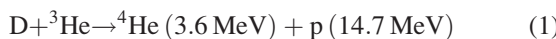


FIG. 1. WRF proton spectrometer setup for measurements of the D^3He-p spectrum in different directions at the NIF. Polar and equatorial WRFs have the same distance (50 cm) and displacement from the DIM axis ($\pm 13.6^\circ$). Typical capsule dimensions shown at right, the plastic shell ($\rho = 1.08 \text{ g/cm}^3$) is filled with a 30:70 atomic mixture of D and ^3He fuel.

II. NIF ASYMMETRY MEASUREMENTS

Charged-particle measurements of ρR asymmetries have previously been used at the OMEGA laser facility¹⁷ for spherically symmetric direct-drive implosions^{18,19} and direct-drive implosions with induced asymmetries.²⁰ Extending this technique to NIF has been discussed.²¹ The reaction



is used. The high-energy proton escapes implosions with $\rho R \lesssim 300 \text{ mg/cm}^2$. This limit is set by the charged-particle stopping power in plasmas.²² During an implosion, a strong shock wave runs ahead of the imploding shell and rebounds at the origin several hundred ps before the main compression phase, creating densities and temperatures high enough for a brief period of fusion burn (shock bang)^{23,24} that produces protons via Eq. (1). Recent work has inferred a shock-compression bang-time differential of 400–800 ps for these implosions,²⁵ which will be measured more precisely in the future.²⁶

For the implosions^{14,27} studied at the NIF, surrogate²⁸ CH capsules filled with D_2 and ^3He gas converge to $R \sim 200$ –300 μm by the shock bang time (compared to an initial inner radius of $\sim 900 \mu\text{m}$), at which point the total ρR has reached ~ 60 –120 mg/cm^2 . During the main compression burn, $\rho R \gg 300 \text{ mg/cm}^2$, so the D^3He-p are ranged out.

The protons are measured with compact Wedge Range Filter (WRF) spectrometers.^{29–31} Multiple spectrometers are fielded in the (0,0) polar Diagnostic Instrument Manipulator³² (DIM) and in an equatorial DIM, (90,78), as shown in Fig. 1. Each WRF spectrometer is a 5 cm diameter “can,” with an active area approximately $2 \times 2 \text{ cm}$, placed 50 cm from target-chamber center (TCC). WRFs in the polar DIM view the implosion through the laser entrance hole (LEH). The equatorial WRFs measure protons through the hohlraum wall which

causes additional downshift; the results are corrected for this energy loss in the wall using cold-matter stopping powers³³ and known material thicknesses.³⁴ Other materials, such as the capsule “tent” and hohlraum gas fill, are negligible.³⁵ One or two spectrometers can be fielded at a displacement of $\pm 13.6^\circ$ from the axis for both DIMs.

In these surrogate NIF implosions, differences in the mean shock proton energy between the polar and hohlraum-corrected equatorial spectra are routinely observed. Fig. 2 shows spectra measured on the pole and equator for shot N101218, which had a large asymmetry induced by a known capsule offset. On this shot, the polar WRF measured a lower

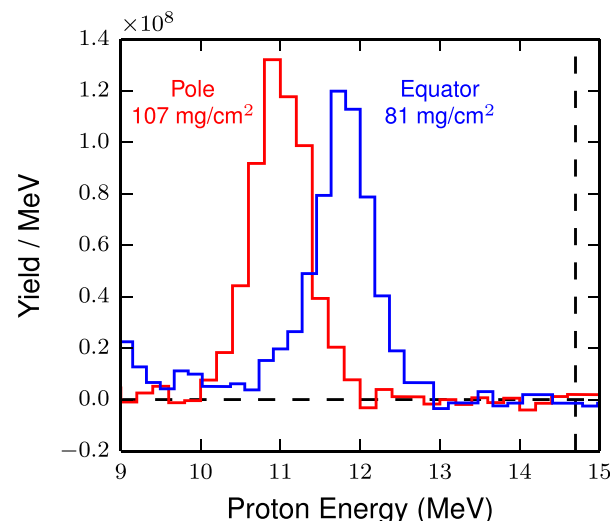


FIG. 2. Sample WRF proton spectra from NIF shot N101218 on the pole (red) and equator (blue, after hohlraum wall correction). The D^3He-p birth energy of 14.7 MeV is also shown (vertical dashed line). From the downshift of the measured spectra, ρR values of $107 \pm 2_{\text{ran}} \pm 6_{\text{sys}} \text{ mg/cm}^2$ (pole) and $81 \pm 2_{\text{ran}} \pm 6_{\text{sys}} \text{ mg/cm}^2$ (equator) were inferred.

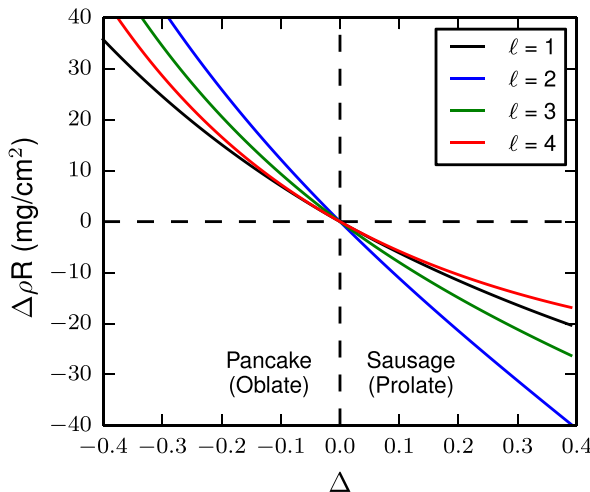


FIG. 3. Observable ρR asymmetry (pole – equator) versus mode perturbation amplitude Δ for $m=0$ modes with $\ell = 1, 2, 3, 4$ with the shell average $\bar{R} = 250 \mu\text{m}$ (average $\rho R = 89 \text{ mg/cm}^2$) corresponding to N101218. For a given perturbation Δ , a $\ell = 2$ mode (blue curve) causes the largest observable asymmetry.

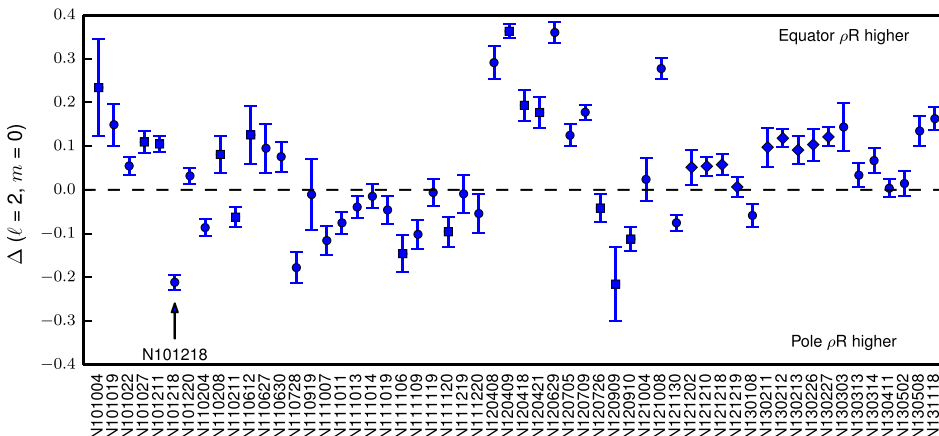
shock proton energy, thus the polar ρR is higher: 107 mg/cm^2 versus 81 on the equator, for a difference $\Delta \rho R$ of 26 mg/cm^2 .

These spectral differences in the polar and equatorial spectrometry data cannot be attributed to electromagnetic fields. First, prior work has demonstrated that electric fields generated in indirect-drive targets decay early within the laser drive,^{36,37} while these data are obtained after the laser is turned off. Transverse magnetic fields exist near the laser-entrance hole³⁸ for these implosions; the magnetic fields cause asymmetries in proton flux but do not affect the proton mean energy and thus the inferred ρR and shell R_{cm} are unaffected. The spectral differences must be caused by differences in the energy slowing of the protons exiting the implosion and thus in the implosion ρR .

Low-mode asymmetries can be modeled by spherical harmonic perturbations of the imploding shell's center-of-mass radius as

$$R_{cm}(\theta, \phi) = \bar{R}[1 + \Delta \times \alpha e^{im\phi} P_\ell^m(\cos \theta)], \quad (2)$$

where θ and ϕ are the polar and azimuthal angles, respectively, \bar{R} is the unperturbed shell radius, Δ is the fractional asymmetry amplitude, α is the normalization factor,³⁹ and



P_ℓ^m is an associated Legendre polynomial. This shape analysis using the radius enables direct comparison to x-ray metrics, which are typically given as fractional Legendre amplitudes (i.e., Δ). As we do not know *a priori* whether polar or azimuthal modes (or both) are responsible for observed differences between the two lines of sight (see Fig. 1), both are included here for generality.

Using a simple 1-D model, ρR and R_{cm} are simultaneously inferred from the proton energy measurement using a mass profile self-consistently converged to relate R_{cm} , ρR , and measured proton energy. Multiple proton measurements of R_{cm} at various θ, ϕ are then fit with the functional form for $R_{cm}(\theta, \phi)$ (Eq. (2)).⁴⁰ Since the asymmetries are manifested as a relative difference between the measurements, only “random” or statistical uncertainties are retained in this analysis. The polar-equatorial geometry would suggest the assumption of a $\ell = 2, m = 0$ mode asymmetry. However, with limited WRF lines of sight, we cannot differentiate between various modes. For instance, in Fig. 3, the difference in ρR between the polar and equatorial WRFs for assumed polar ($m=0$) modes with $\ell = 1, 2, 3, 4$ are plotted. Modes 2 and 4 are known to be prevalent in these NIF implosions,⁹ and the potential for deleterious mode 1 asymmetries has been recognized.^{41,42}

For a given Δ , the observable difference in ρR is maximized if the mode is a P_2 (i.e., $\ell = 2, m = 0$). Fig. 3 shows that this technique is half as sensitive to modes $\ell = 1, 3, 4$ with the current detector geometry (Fig. 1). While we cannot differentiate between a $\ell = 2$ mode and a $\ell = 1$ mode with twice the perturbation amplitude, due to the limited diagnostic lines of sight,⁴³ for a difference in ρR between pole and equator this work assumes a $\ell = 2$ mode, which minimizes the inferred Δ . The asymmetry amplitude Δ is plotted for all shots in this work in Fig. 4, with 1σ error bars.

The ρR asymmetries do not have systematic direction, i.e., approximately the same number of shots have a higher polar ρR (negative Δ) as the number of shots with higher equator ρR (positive Δ). Only 20%–30% of the shots are consistent within error bars with a symmetric ($\Delta = 0$) implosion.

III. COMPARISON TO STAGNATION X-RAY ASYMMETRY

We can compare this work to compression x-ray self-emission imaging^{14,44} at $CR \sim 20$. The dataset plotted in

FIG. 4. Mode amplitude Δ (see Eq. (2)) for all NIF shots with polar and equatorial WRF data since 2010 (numerous tuning changes over the campaigns resulted in large differences in shot-to-shot symmetry). Shot numbers are displayed below. Displayed error bars are 1σ . Positive values represent higher ρR on the equator. Shot N101218 (also shown in Fig. 2) is specifically annotated. Shots used in Fig. 5 denoted by square markers, and in Fig. 6 by diamond markers.

Fig. 4 is reduced to experiments with very good stagnation azimuthal symmetry as measured by polar-view x-ray imaging ($m_2/m_0 < 10\%$ and $m_4/m_0 < 15\%$) to reduce effects of m modes and with a small polar mode-4 asymmetry ($P_4/P_0 < 15\%$). For shots satisfying these cuts, the assumption of a P_2 -dominated asymmetry in our measurement is valid. In Fig. 4, these shots are denoted by the square markers. The ρR P_2 data are compared directly to the stagnation x-ray symmetry measurement in Fig. 5. As the x-ray metric is generally referred to in literature as P_2/P_0 , we follow that convention here; for the WRF measurement this is equivalent to Δ in Fig. 4.

In the data, we see a positive correlation between the $\ell = 2$ mode amplitude inferred from the shock ρR and the stagnation x-ray emission shape. A linear fit to the data provides a slope of 0.6 ± 0.1 .

To further investigate this, we generate a second dataset using recently-developed in-flight x-ray radiography of the imploding shell, which measures the shape at a similar time in the implosion as the ρR measurements.⁹ These shots correspond to a subset of Fig. 4 denoted by diamond markers. The radiography data show significant $\ell = 2$ and $\ell = 4$ modes. The radiography requires large oppositely-placed patches on the hohlraum wall, which induces a large $m = 2$ asymmetry roughly aligned with the equatorial WRF line of sight. With limited lines of sight, this generates an unconstrained problem for this analysis. However, if the radiography-measured amplitudes for $\ell = 2$ and $\ell = 4$ modes at $CR \sim 4$ are used with a superimposed azimuthal mode $\Delta \sin(\theta) \cos(m\phi + \phi_0)$ with $m = 2$, ϕ_0 aligned with the WRF equatorial view, and Δ a free parameter, the in-flight azimuthal shape (m_2) is then characterized.

The results of this analysis are shown in Fig. 6, compared to the stagnation x-ray emission shape as in Fig. 5. Again positive correlation is observed with a slope of approximately unity (0.82 ± 0.25). The positive correlation between the shock and compression asymmetries means that

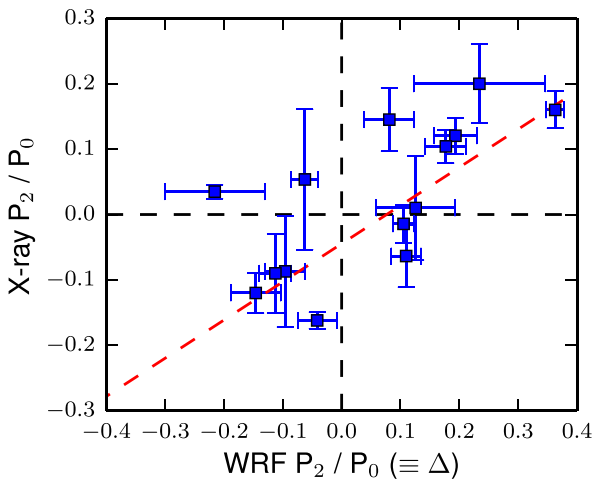


FIG. 5. Mode $\ell = 2$ amplitude from these measurements (abscissa) versus stagnation x-ray core emission shape. A linear fit (dashed red line) to the data has slope 0.6 ± 0.1 and intercept -0.04 ± 0.02 . The data have a weighted Pearson correlation coefficient $p = 0.68$.

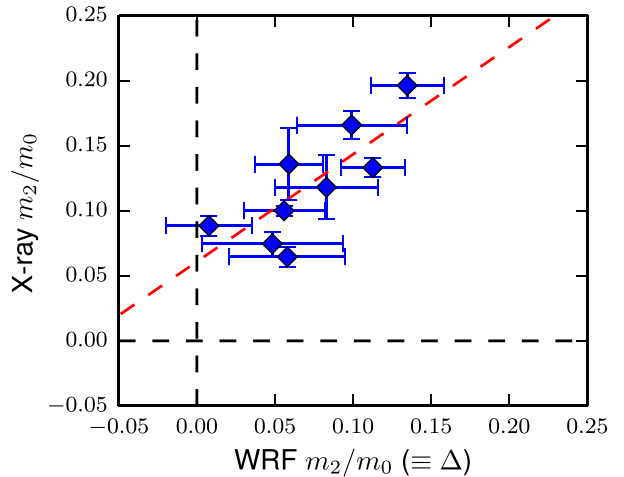


FIG. 6. Azimuthal mode amplitude inferred for experiments with in-flight x-ray imaging: this work (abscissa) versus stagnation x-ray core shape. A linear fit (dashed red line) to the data has slope 0.82 ± 0.25 and intercept 0.06 ± 0.02 . The data have a weighted Pearson correlation coefficient $p = 0.78$.

the asymmetry maintains its phase during deceleration (i.e., a prolate in-flight implosions has a prolate stagnated shape).

In Figs. 5 and 6, as the abscissa is the shock-bang-time asymmetry and the ordinate is the compression-bang-time asymmetry, the slope in the data corresponds directly to the amplitude of the asymmetry at compression relative to shock, i.e., the growth factor between these times. In both data sets (Figs. 5 and 6), the slope being ≤ 1 indicates a lack of growth in apparent mode amplitude between shock ($CR \sim 4$) and compression ($CR \sim 20$) phases. To explore this further, we consider several models for asymmetry growth of a radial $\ell = 2$ perturbation. The simplest is Bell-Plesset, a model for asymmetric incompressible flows in spherical compression,⁴⁵ which predicts a simple convergence scaling $\Delta \propto (CR - 1)$. For ICF, modified Bell-Plesset theory for compressible flows⁴⁶ is more appropriate. Finally, we also consider typical 2-D radiation hydrodynamics simulations of asymmetrically driven surrogate implosions using HYDRA.⁴⁷ The expected growth factors between the shock and compression times using these models are summarized in Table I.

The growth factor corresponds directly to an expected slope in Figs. 5 and 6, clearly inconsistent with the data for all models. This is in contrast to the previous experiments showing that the Bell-Plesset model holds for low-mode asymmetry growth between shock and compression in direct-drive OMEGA implosions.^{19,20}

TABLE I. Growth factors from shock to compression for several models.

Model	Growth
Bell-Plesset	$\sim 5\times$
Compressible Bell-Plesset	$\sim 3\times$
2D HYDRA (picket and trough) ^a	$\sim -14\times$
2D HYDRA (peak) ^b	$\sim 3\times$

^a10% flux asymmetry applied during the first picket and trough.

^b10% flux asymmetry applied during the peak power.

The most plausible explanation for this result is that the stagnation x-ray emission shape asymmetries do not represent (i.e., are smaller than) the ρR asymmetries at that time. A lack of correspondence between stagnation x-ray and ρR asymmetries has been seen in recent computational studies,^{12,48–51} in indirect-drive OMEGA experiments,⁵² and in the 2-D HYDRA simulations used for Table I. This interpretation is consistent with the results of DT-layered cryogenic implosions at NIF, where neutron metrics^{53–55} show very large ρR asymmetries, of order $2 – 3 \times$ variation between lines of sight at compression, while the x-ray core shape is much closer to symmetric.⁵⁶

The growth models considered in Table I implicitly assume efficient conversion of the imploding shell's kinetic energy into stagnated thermal energy. If significant residual kinetic energy exists at stagnation, for example, through non-radial flows or turbulent motion, then we would not expect the growth models to be valid. Whether a growth factor ~ 1 is consistent with this hypothesis could be investigated with 3D radiation-hydrodynamics simulations.

Another consideration is scenarios which cause ρR asymmetries but not shape asymmetries, such as variations in shell remaining mass or density in addition to convergence (shape). These scenarios would still cause significant performance degradation, and will be investigated using in-flight x-ray radiography⁹ to complement this technique. Finally, the presence of $\ell = 1$ modes could affect the shock ρR but not be apparent in x-ray stagnation imaging; however we note that the asymmetry magnitudes in this work are consistent with in-flight x-ray radiography,⁹ suggesting that $\ell = 1$ is not dominant. This could be verified with dedicated shots inducing $\ell = 1$ modes in these implosions, similar to recent experiments with DT fuel.^{41,42}

Finally, the effects of bulk fuel velocity and scattering are small for this technique (see the Appendix).

IV. COASTING INTERPRETATION

The cause of the large variation in observed asymmetries, both in magnitude and sign, has also been investigated. As in Fig. 5, we control for variation in other asymmetry modes by selecting shots with $m_2/m_0 < 10\%$, $m_4/m_0 < 15\%$, and $P_4/P_0 < 15\%$. For this data set, a significant anti-correlation has been found with the implosion coasting time, which is the difference in time between the end of the laser drive and the peak nuclear production. The data are shown in Fig. 7. The anti-correlation means that the implosions are more prolate (sausaged) for short-coast (extended drive) pulses. This sensitivity suggests that the asymmetries result from asymmetries in the flux during peak drive. The trend with coasting, and an apparent change in asymmetry sign near a coast time ~ 1.75 ns, means that the peak flux has a time-varying asymmetry. The P_2 flux asymmetry during the peak drive depends on the relative strength of the inner and outer beams (cone fraction), the wavelength separation between beams ($\delta\lambda$), and thus on the cross-beam energy transfer which has an additional complex dependence on the hohlraum plasma conditions.

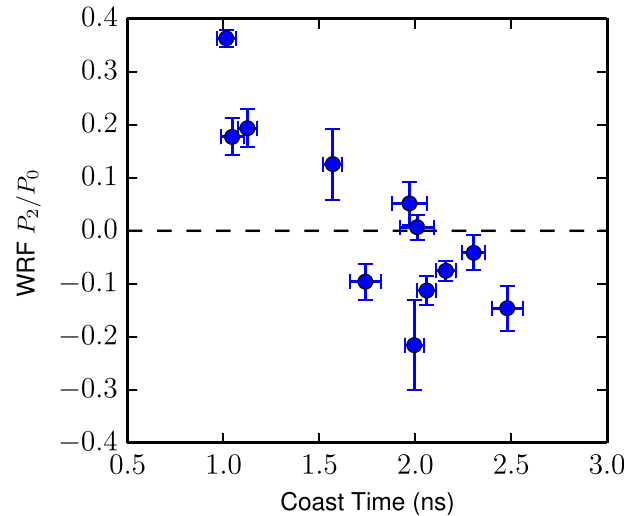


FIG. 7. WRF-measured P_2/P_0 mode amplitude versus implosion coasting time.

V. CONCLUSION

In conclusion, implosion ρR asymmetries are clearly observed at the shock-bang time in D³He surrogate experiments at the NIF. This technique is unique because it uses charged particles to probe ρR asymmetries at the shock bang several hundred ps before implosion stagnation, corresponding to a convergence ratio of $\sim 3 – 5$ and occurring just before peak implosion velocity, thus isolating acceleration-phase asymmetry growth. The observed asymmetries are interpreted as a $\ell = 2 (P_2)$ asymmetry in shape, with the data routinely showing asymmetry magnitudes $\gtrsim 10\%$ at this time. These asymmetries would degrade performance later in time during stagnation, with growth factors $\gtrsim 3\times$ predicted by several models. However, when comparing these measured asymmetries to the x-ray stagnation emission shape, a lack of growth is observed in apparent asymmetry mode amplitude, in contrast to the expected $\gtrsim 3\times$ growth. This suggests the x-ray stagnation emission shape does not accurately reflect the stagnation shell (ρR) shape or possibly that significant residual kinetic energy exists. Finally, the observed variations in asymmetry magnitude and sign are partly explained by an anti-correlation with the implosion coasting time, suggesting that a significant time-dependent asymmetry in the peak flux drives the observed implosion asymmetries. Such a time-dependent $\ell = 2$ asymmetry could be caused by the cross-beam energy transfer between the inner and outer beams varying during the main pulse. Importantly, with several techniques now available for measuring the symmetry over the entire implosion evolution from $CR = 1 \rightarrow 20$, these observed asymmetries can be studied and mitigated, as necessary for ignition on the NIF.

ACKNOWLEDGMENTS

We thank the operations crews and engineering staff at NIF for supporting these experiments, and M. McKernan, M. Cairel, and M. Valadez for their work processing the CR-39.

This work is part of the first author's Ph.D. thesis and was supported in part by the U.S. DoE (Grant No. DE-NA0001857, DE-FC52-08NA28752), LLNL (No. B597367),

LLE (No. 415935-G), the Fusion Science Center at the University of Rochester (No. 524431), and the National Laser Users Facility (No. DE-NA0002035). This material is based upon work supported by the National Science Foundation Graduate Research Fellowship Program under Grant No. 1122374.

APPENDIX A: BULK VELOCITY EFFECTS

Bulk velocity of the fuel creates Doppler shifts in the fusion products due to center-of-mass motion of the reacting ions. The mean D³He proton birth energy $E_p(T_i)$ is used to calculate the initial velocity in the center-of-mass frame: $\gamma_0 = 1 + E_p/(m_p c^2)$ and $v_0 = c \sqrt{1 - \gamma_0^{-2}}$. For a given bulk velocity v_b in the detector direction the velocities add relativistically:

$$v' = \frac{v_0 + v_b}{1 + v_0 v_b / c^2}, \quad \gamma' = 1 / \sqrt{1 - (v'/c)^2}, \quad (\text{A1})$$

with the Doppler shifted energy given by

$$E'_p = (\gamma' - 1)m_p c^2, \quad \Delta E_p = E'_p - E_p, \quad (\text{A2})$$

where ΔE_p is the energy shift due to the bulk velocity. Using relativistic kinematics⁵⁷ and the parameterized cross-section,⁵⁸ ΔE_p is calculated and shown in Fig. 8(a) as a function of the bulk velocity.

If the burning fuel has a bulk velocity in the direction of one of the detectors, the higher (lower) initial proton energy results in a higher (lower) final proton energy, which results in a lower (higher) inferred ρR . This is shown in Fig. 8(b). Since the polar and equatorial detectors are approximately orthogonal, a bulk fuel velocity towards one DIM will not cause an energy shift towards the other, meaning that the shift in inferred ρR due to the velocity causes an apparent asymmetry, which is shown in Fig. 8(c).

As the protons are created by the shock coalescence and burn, any net fuel velocity would be caused by an asymmetry in the converging shock. The most comparable scenario are shock-driven “exploding pusher” implosions, in which all of the nuclear yield is produced by a single strong shock. The shock strength is much higher in exploding pushers than in the low-adiabat surrogate implosions used in this work, and thus the bulk fuel velocity in exploding pushers can be taken as an upper limit.

In a D³He exploding pusher on NIF, the proton energy uniformity was observed to be ± 75 keV between the pole and equator,⁵⁹ corresponding to ≤ 150 km/s bulk fuel velocity if attributed entirely to Doppler shifts. In DT exploding pushers,⁶⁰ DT-n Doppler shifts were observed corresponding to fuel velocities up to 200 km/s. For velocities up to ± 200 km/s, the apparent asymmetry caused by the proton Doppler shift is ± 0.04 in Δ . As this is much smaller than the observed asymmetries, which have $\Delta = 0.1 - 0.2$ routinely, plausible bulk fuel velocity Doppler shifts cannot cause the observed asymmetries, but may be responsible for some of the observed shot-to-shot scatter in Figs. 5 and 6.

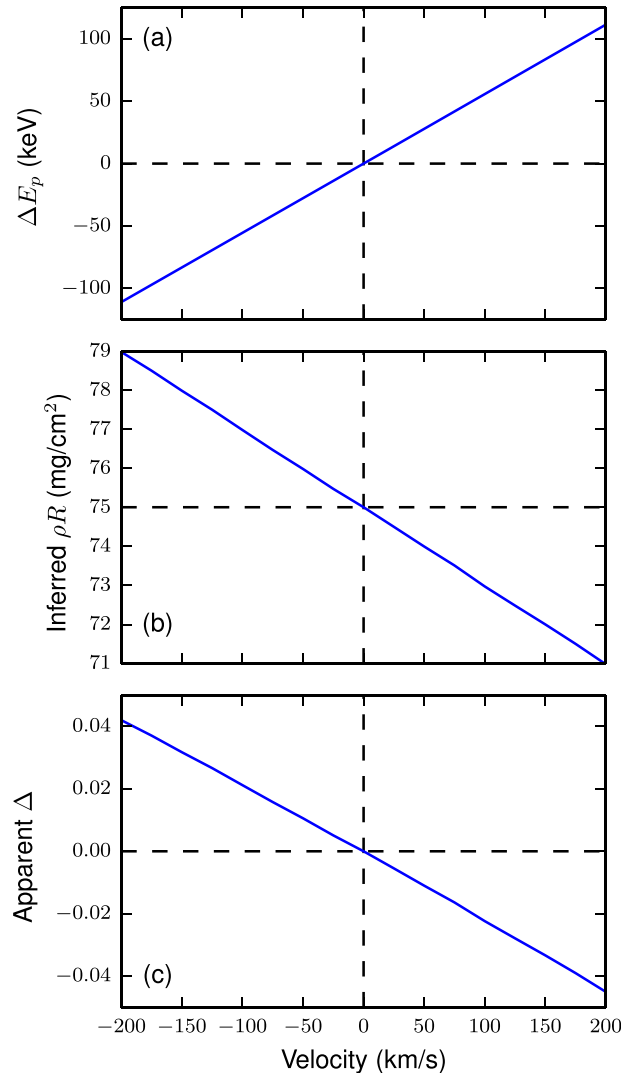


FIG. 8. (a) D³He proton birth energy shift as a function of bulk fuel velocity. (b) For an actual $\rho R = 75$ mg/cm², the apparent ρR due to birth energy shift as a function of velocity. (c) The apparent asymmetry amplitude (Δ) as a function of bulk velocity.

APPENDIX B: SCATTERING EFFECTS

As the protons traverse material, they undergo collisions. Rutherford scattering off of atomic nuclei can produce large-angle deflections, which could potentially mask asymmetries via scattering in materials surrounding the target. The differential cross section is

$$\frac{d\sigma}{d\Omega} = \frac{b_{90}^2}{4} \frac{1}{\sin^4(\theta/2)}, \quad (\text{B1})$$

with

$$b_{90} = \frac{Z_1 Z_2 e^2}{4\pi\epsilon_0} \frac{1}{m_\mu v_{rel}^2}. \quad (\text{B2})$$

The protons are energetic, so v_{rel} is relatively high, leading to a suppression of scattering effects as the cross section $\propto v_{rel}^{-4}$. Additionally, large-angle scattering is suppressed by the $\sin^{-4}(\theta/2)$ dependence. This leads to large-angle scattering being a small effect, which can be verified with the TRIM Monte Carlo code.³³

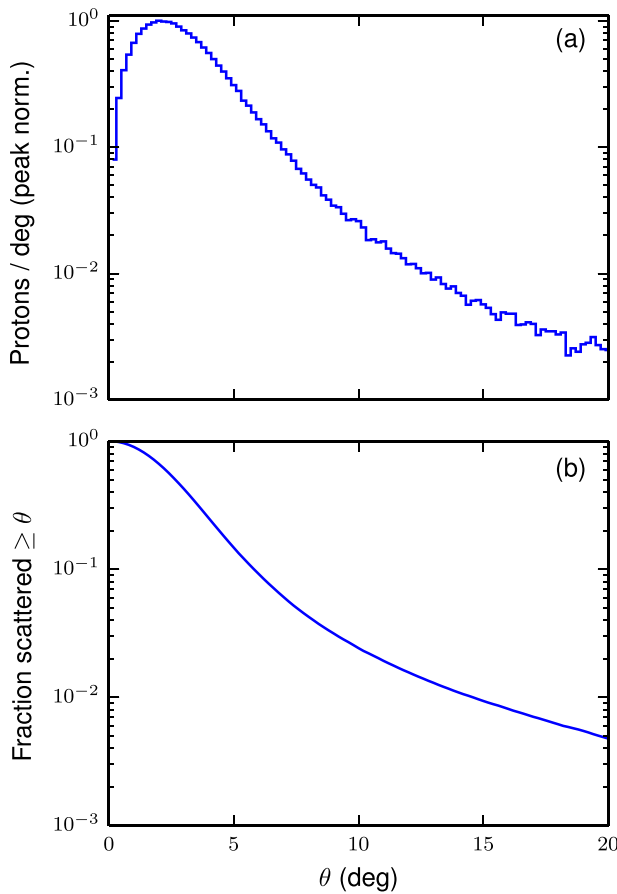


FIG. 9. Proton scattering in a typical hohlraum wall ($30\ \mu\text{m}$ of Au and $74\ \mu\text{m}$ of Al). (a) The proton angular distribution after transiting the wall. (b) The fraction of protons scattered more than θ versus θ .

Most of the hohlraum is surrounded by significantly thicker material, such as a diagnostic band, while the equatorial line-of-sight for the WRFs looks through a thinner region. While protons going through the thicker regions of the wall may undergo large-angle scattering into the detector solid angle, their energies will be much lower than the protons exiting the hohlraum through the thin region, and thus these protons will not be counted in the analysis.

The effect of scattering on protons transiting the nominal hohlraum wall ($30\ \mu\text{m}$ of Au and $74\ \mu\text{m}$ of Al) near the line-of-sight is evaluated with TRIM, and shown in Fig. 9. Most of the scattering occurs in the Au wall due to the Z^2 dependence (Eqs. (B1) and (B2)). Fig. 9(a) shows the angular distribution of protons after the wall for a typical initial energy $E_p = 12\ \text{MeV}$. The distribution peaks $\sim 2^\circ$ scattering angle. Fig. 9(b) shows the distribution as the fraction of protons scattered with angle greater than θ . The TRIM calculation shows that $\sim 90\%$ of protons scatter less than 5° in the wall, and $\sim 98\%$ scatter less than 10° . This means that we expect high-mode asymmetries to be masked by scattering, but low-mode asymmetries, the focus of this paper, are unaffected.

¹J. Nuckolls, L. Wood, A. Thiessen, and G. Zimmerman, *Nature* **239**, 139 (1972).

²J. Lindl, *Phys. Plasmas* **2**, 3933 (1995).

³G. Miller, E. Moses, and C. Wuest, *Nucl. Fusion* **44**, S228 (2004).

⁴S. W. Haan, S. M. Pollaine, J. D. Lindl, L. J. Suter, R. L. Berger, L. V. Powers, W. E. Alley, P. A. Amendt, J. A. Futterman, W. K. Levedahl, M. D. Rosen, D. P. Rowley, R. A. Sacks, A. I. Shestakov, G. L. Strobel, M. Tabak, S. V. Weber, G. B. Zimmerman, W. J. Krauser, D. C. Wilson, S. V. Coggeshall, D. B. Harris, N. M. Hoffman, and B. H. Wilde, *Phys. Plasmas* **2**, 2480 (1995).

⁵S. Atzeni, *Europhys. Lett.* **11**, 639 (1990).

⁶S. W. Haan, J. D. Lindl, D. A. Callahan, D. S. Clark, J. D. Salmonson, B. A. Hammel, L. J. Atherton, R. C. Cook, M. J. Edwards, S. Glenzer, A. V. Hamza, S. P. Hatchett, M. C. Herrmann, D. E. Hinkel, D. D. Ho, H. Huang, O. S. Jones, J. Kline, G. Kyrala, O. L. Landen, B. J. MacGowan, M. M. Marinak, D. D. Meyerhofer, J. L. Milovich, K. A. Moreno, E. I. Moses, D. H. Munro, A. Nikroo, R. E. Olson, K. Peterson, S. M. Pollaine, J. E. Ralph, H. F. Robey, B. K. Spears, P. T. Springer, L. J. Suter, C. A. Thomas, R. P. Town, R. Vesey, S. V. Weber, H. L. Wilkens, and D. C. Wilson, *Phys. Plasmas* **18**, 051001 (2011).

⁷S. H. Glenzer, B. J. MacGowan, P. Michel, N. B. Meezan, L. J. Suter, S. N. Dixit, J. L. Kline, G. A. Kyrala, D. K. Bradley, D. A. Callahan, E. L. Dewald, L. Divol, E. Dzenitis, M. J. Edwards, A. V. Hamza, C. A. Haynam, D. E. Hinkel, D. H. Kalantar, J. D. Kilkenny, O. L. Landen, J. D. Lindl, S. LePape, J. D. Moody, A. Nikroo, T. Parham, M. B. Schneider, R. P. J. Town, P. Wegner, K. Widmann, P. Whitman, B. K. F. Young, B. Van Wonterghem, L. J. Atherton, and E. I. Moses, *Science* **327**, 1228 (2010).

⁸O. L. Landen, T. R. Boehly, D. K. Bradley, D. G. Braun, D. A. Callahan, P. M. Celliers, G. W. Collins, E. L. Dewald, L. Divol, S. H. Glenzer, A. Hamza, D. G. Hicks, N. Hoffman, N. Izumi, O. S. Jones, R. K. Kirkwood, G. A. Kyrala, P. Michel, J. Milovich, D. H. Munro, A. Nikroo, R. E. Olson, H. F. Robey, B. K. Spears, C. A. Thomas, S. V. Weber, D. C. Wilson, M. M. Marinak, L. J. Suter, B. A. Hammel, D. D. Meyerhofer, J. Atherton, J. Edwards, S. W. Haan, J. D. Lindl, B. J. MacGowan, and E. I. Moses, *Phys. Plasmas* **17**, 056301 (2010).

⁹J. R. Rygg, O. S. Jones, J. E. Field, M. A. Barrios, L. R. Benedetti, G. W. Collins, D. C. Eder, M. J. Edwards, J. L. Kline, J. J. Kroll, O. L. Landen, T. Ma, A. Pak, J. L. Peterson, K. Raman, R. P. J. Town, and D. K. Bradley, *Phys. Rev. Lett.* **112**, 195001 (2014).

¹⁰E. L. Dewald, J. Milovich, C. Thomas, J. Kline, C. Sorce, S. Glenn, and O. L. Landen, *Phys. Plasmas* **18**, 092703 (2011).

¹¹E. L. Dewald, J. L. Milovich, P. Michel, O. L. Landen, J. L. Kline, S. Glenn, O. Jones, D. H. Kalantar, A. Pak, H. F. Robey, G. A. Kyrala, L. Divol, L. R. Benedetti, J. Holder, K. Widmann, A. Moore, M. B. Schneider, T. Döppner, R. Tommasini, D. K. Bradley, P. Bell, B. Ehrlrich, C. A. Thomas, M. Shaw, C. Widmayer, D. A. Callahan, N. B. Meezan, R. P. J. Town, A. Hamza, B. Dzenitis, A. Nikroo, K. Moreno, B. Van Wonterghem, A. J. Mackinnon, S. H. Glenzer, B. J. MacGowan, J. D. Kilkenny, M. J. Edwards, L. J. Atherton, and E. I. Moses, *Phys. Rev. Lett.* **111**, 235001 (2013).

¹²R. P. J. Town, D. K. Bradley, A. Kritcher, O. S. Jones, J. R. Rygg, R. Tommasini, M. Barrios, L. R. Benedetti, L. F. Berzak Hopkins, P. M. Celliers, T. Döppner, E. L. Dewald, D. C. Eder, J. E. Field, S. M. Glenn, N. Izumi, S. W. Haan, S. F. Khan, J. L. Kline, G. A. Kyrala, T. Ma, J. L. Milovich, J. D. Moody, S. R. Nagel, A. Pak, J. L. Peterson, H. F. Robey, J. S. Ross, R. H. H. Scott, B. K. Spears, M. J. Edwards, J. D. Kilkenny, and O. L. Landen, *Phys. Plasmas* **21**, 056313 (2014).

¹³J. D. Moody, D. A. Callahan, D. E. Hinkel, P. A. Amendt, K. L. Baker, D. Bradley, P. M. Celliers, E. L. Dewald, L. Divol, T. Döppner, D. C. Eder, M. J. Edwards, O. Jones, S. W. Haan, D. Ho, L. B. Hopkins, N. Izumi, D. Kalantar, R. L. Kauffman, J. D. Kilkenny, O. Landen, B. Lasinski, S. LePape, T. Ma, B. J. MacGowan, S. A. McLaren, A. J. Mackinnon, D. Meeker, N. Meezan, P. Michel, J. L. Milovich, D. Munro, A. E. Pak, M. Rosen, J. Ralph, H. F. Robey, J. S. Ross, M. B. Schneider, D. Strozzi, E. Storm, C. Thomas, R. P. J. Town, K. L. Widmann, J. Kline, G. Kyrala, A. Nikroo, T. Boehly, A. S. Moore, and S. H. Glenzer, *Phys. Plasmas* **21**, 056317 (2014).

¹⁴G. A. Kyrala, S. Dixit, S. Glenzer, D. Kalantar, D. Bradley, N. Izumi, N. Meezan, O. L. Landen, D. Callahan, S. V. Weber, J. P. Holder, S. Glenn, M. J. Edwards, P. Bell, J. Kimbrough, J. Koch, R. Prasad, L. Suter, J. L. Kline, and J. Kilkenny, *Rev. Sci. Instrum.* **81**, 10E316 (2010).

¹⁵S. H. Glenzer, B. K. Spears, M. J. Edwards, E. T. Alger, R. L. Berger, D. L. Bleuel, D. K. Bradley, J. A. Caggiano, D. A. Callahan, C. Castro, D. T. Casey, C. Choate, D. S. Clark, C. J. Cerjan, G. W. Collins, E. L. Dewald, J.-M. G. D. Nicola, P. D. Nicola, L. Divol, S. N. Dixit, T. Döppner, R. Dylla-Spears, E. G. Dzenitis, J. E. Fair, L. J. A. Frenje, M. G. Johnson, E. Giraldez, V. Glebov, S. M. Glenn, S. W. Haan, B. A. Hammel, S. P. Hatchett II, C. A. Haynam, R. F. Heeter, G. M. Heestand, H. W. Herrmann,

- D. G. Hicks, D. M. Holunga, J. B. Horner, H. Huang, N. Izumi, O. S. Jones, D. H. Kalantar, J. D. Kilkenny, R. K. Kirkwood, J. L. Kline, J. P. Knauer, B. Kozioziemski, A. L. Kritcher, J. J. Kroll, G. A. Kyrala, K. N. LaFortune, O. L. Landen, D. W. Larson, R. J. Leeper, S. L. Pape, J. D. Lindl, T. Ma, A. J. Mackinnon, A. G. MacPhee, E. Mapoles, P. W. McKenty, N. B. Meezan, P. Michel, J. L. Milovich, J. D. Moody, A. S. Moore, M. Moran, K. A. Moreno, D. H. Munro, B. R. Nathan, A. Nikroo, R. E. Olson, C. D. Orth, A. Pak, P. K. Patel, T. Parham, R. Petrasco, J. E. Ralph, H. Rinderknecht, S. P. Regan, H. F. Robey, J. S. Ross, J. D. Salmonson, C. Sangster, J. Sater, M. B. Schneider, F. H. Sguin, M. J. Shaw, M. J. Shoup, P. T. Springer, W. Stoeffl, L. J. Suter, C. A. Thomas, R. P. J. Town, C. Walters, S. V. Weber, P. J. Wegner, C. Widmayer, P. K. Whitman, K. Widmann, D. C. Wilson, B. M. V. Wonteghem, B. J. MacGowan, L. J. Atherton, and E. I. Moses, *Plasma Phys. Controlled Fusion* **54**, 045013 (2012).
- ¹⁶G. P. Grim, N. Guler, F. E. Merrill, G. L. Morgan, C. R. Danly, P. L. Volegov, C. H. Wilde, D. C. Wilson, D. S. Clark, D. E. Hinkel, O. S. Jones, K. S. Raman, N. Izumi, D. N. Fittinghoff, O. B. Drury, E. T. Alger, P. A. Arnold, R. C. Ashabrunner, L. J. Atherton, M. A. Barrios, S. Batha, P. M. Bell, L. R. Benedetti, R. L. Berger, L. A. Bernstein, L. V. Berzins, R. Betti, S. D. Bhandarkar, R. M. Bionta, D. L. Bleuel, T. R. Boehly, E. J. Bond, M. W. Bowers, D. K. Bradley, G. K. Brunton, R. A. Buckles, S. C. Burkhardt, R. F. Burr, J. A. Caggiano, D. A. Callahan, D. T. Casey, C. Castro, P. M. Celliers, C. J. Cerjan, G. A. Chandler, C. Choate, S. J. Cohen, G. W. Collins, G. W. Cooper, J. R. Cox, J. R. Cradick, P. S. Datte, E. L. Dewald, P. Di Nicola, J. M. Di Nicola, L. Divol, S. N. Dixit, R. Dylla-Spears, E. G. Dzenitis, M. J. Eckart, D. C. Eder, D. H. Edgell, M. J. Edwards, J. H. Eggert, R. B. Ehrlich, G. V. Erbert, J. Fair, D. R. Farley, B. Felker, R. J. Fortner, J. A. Frenje, G. Frieders, S. Friedrich, M. Gatu-Johnson, C. R. Gibson, E. Giraldez, V. Y. Glebov, S. M. Glenn, S. H. Glenzer, G. Gururangan, S. W. Haan, K. D. Hahn, B. A. Hammel, A. V. Hamza, E. P. Hartouni, R. Hatarik, S. P. Hatchett, C. Haynam, M. R. Hermann, H. W. Herrmann, D. G. Hicks, J. P. Holder, D. M. Holunga, J. B. Horner, W. W. Hsing, H. Huang, M. C. Jackson, K. S. Jancaitis, D. H. Kalantar, R. L. Kauffman, M. I. Kauffman, S. F. Khan, J. D. Kilkenny, J. R. Kimbrough, R. Kirkwood, J. L. Kline, J. P. Knauer, K. M. Knittel, J. A. Koch, T. R. Kohut, B. J. Kozioziemski, K. Krauter, G. W. Krauter, A. L. Kritcher, J. Kroll, G. A. Kyrala, K. N. L. Fortune, G. LaCaille, L. J. Lagin, T. A. Land, O. L. Landen, D. W. Larson, D. A. Latray, R. J. Leeper, T. L. Lewis, S. LePape, J. D. Lindl, R. R. Lowe-Webb, T. Ma, B. J. MacGowan, A. J. MacKinnon, A. G. MacPhee, R. M. Malone, T. N. Malsbury, E. Mapoles, C. D. Marshall, D. G. Mathisen, P. McKenty, J. M. McNaney, N. B. Meezan, P. Michel, J. L. Milovich, J. D. Moody, A. S. Moore, M. J. Moran, K. Moreno, E. I. Moses, D. H. Munro, B. R. Nathan, A. J. Nelson, A. Nikroo, R. E. Olson, C. Orth, A. E. Pak, E. S. Palma, T. G. Parham, P. K. Patel, R. W. Patterson, R. D. Petrasco, R. Prasad, J. E. Ralph, S. P. Regan, H. Rinderknecht, H. F. Robey, G. F. Ross, C. L. Ruiz, F. H. Sguin, J. D. Salmonson, T. C. Sangster, J. D. Sater, R. L. Saunders, M. B. Schneider, D. H. Schneider, M. J. Shaw, N. Simanovskiaia, B. K. Spears, P. T. Springer, C. Stoeckl, W. Stoeffl, L. J. Suter, C. A. Thomas, R. Tommasini, R. P. Town, A. J. Traillie, B. V. Wonteghem, R. J. Wallace, S. Weaver, S. V. Weber, P. J. Wegner, P. K. Whitman, K. Widmann, C. C. Widmayer, R. D. Wood, B. K. Young, R. A. Zacharias, and A. Zylstra, *Phys. Plasmas* **20**, 056320 (2013).
- ¹⁷T. Boehly, D. Brown, R. Craxton, R. Keck, J. Knauer, J. Kelly, T. Kessler, S. Kumpan, S. Loucks, S. Letzring, F. Marshall, R. McCrory, S. Morse, W. Seka, J. Soures, and C. Verdon, *Opt. Commun.* **133**, 495 (1997).
- ¹⁸C. K. Li, F. H. Sguin, J. A. Frenje, R. D. Petrasco, R. Rygg, S. Kurebayashi, B. Schwartz, R. L. Keck, J. A. Delettrez, J. M. Soures, P. W. McKenty, V. N. Goncharov, J. P. Knauer, F. J. Marshall, D. D. Meyerhofer, P. B. Radha, S. P. Regan, T. C. Sangster, W. Seka, and C. Stoeckl, *Phys. Plasmas* **10**, 1919 (2003).
- ¹⁹J. A. Frenje, C. K. Li, F. H. Seguin, J. Deciantis, S. Kurebayashi, J. R. Rygg, R. D. Petrasco, J. Delettrez, V. Y. Glebov, C. Stoeckl, F. J. Marshall, D. D. Meyerhofer, T. C. Sangster, V. A. Smalyuk, and J. M. Soures, *Phys. Plasmas* **11**, 2798 (2004).
- ²⁰C. K. Li, F. H. Seguin, J. A. Frenje, R. D. Petrasco, J. A. Delettrez, P. W. McKenty, T. C. Sangster, R. L. Keck, J. M. Soures, F. J. Marshall, D. D. Meyerhofer, V. N. Goncharov, J. P. Knauer, P. B. Radha, S. P. Regan, and W. Seka, *Phys. Rev. Lett.* **92**, 205001 (2004).
- ²¹R. D. Petrasco, J. A. Frenje, C. K. Li, F. H. Seguin, J. R. Rygg, B. E. Schwartz, S. Kurebayashi, P. B. Radha, C. Stoeckl, J. M. Soures, J. Delettrez, V. Y. Glebov, D. D. Meyerhofer, and T. C. Sangster, *Phys. Rev. Lett.* **90**, 095002 (2003).
- ²²C. Li and R. Petrasco, *Phys. Rev. Lett.* **70**, 3059 (1993).
- ²³G. Guderley, *Luftfahrtforsch* **19**, 302 (1942).
- ²⁴J. R. Rygg, *Shock Convergence and Mix Dynamics in Inertial Confinement Fusion* (Massachusetts Institute of Technology, 2006).
- ²⁵A. B. Zylstra, J. A. Frenje, F. H. Sguin, D. G. Hicks, E. L. Dewald, H. F. Robey, J. R. Rygg, N. B. Meezan, M. J. Rosenberg, H. G. Rinderknecht, S. Friedrich, R. Bionta, R. Olson, J. Atherton, M. Barrios, P. Bell, R. Benedetti, L. Berzak Hopkins, R. Betti, D. Bradley, D. Callahan, D. Casey, G. Collins, S. Dixit, T. Dppner, D. Edgell, M. J. Edwards, M. Gatu Johnson, S. Glenn, S. Glenzer, G. Grim, S. Hatchett, O. Jones, S. Khan, J. Kilkenny, J. Kline, J. Knauer, A. Kritcher, G. Kyrala, O. Landen, S. LePape, C. K. Li, J. Lindl, T. Ma, A. Mackinnon, A. Macphee, M. J.-E. Manuel, D. Meyerhofer, J. Moody, E. Moses, S. R. Nagel, A. Nikroo, A. Pak, T. Parham, R. D. Petrasco, R. Prasad, J. Ralph, M. Rosen, J. S. Ross, T. C. Sangster, S. Sepke, N. Sinenian, H. W. Sio, B. Spears, P. Springer, R. Tommasini, R. Town, S. Weber, D. Wilson, and R. Zacharias, *Phys. Plasmas* **21**, 112701 (2014).
- ²⁶H. G. Rinderknecht, M. G. Johnson, A. B. Zylstra, N. Sinenian, M. J. Rosenberg, J. A. Frenje, C. J. Waugh, C. K. Li, F. H. Sguin, R. D. Petrasco, J. R. Rygg, J. R. Kimbrough, A. MacPhee, G. W. Collins, D. Hicks, A. Mackinnon, P. Bell, R. Bionta, T. Clancy, R. Zacharias, T. Döppner, H. S. Park, S. LePape, O. Landen, N. Meezan, E. I. Moses, V. U. Glebov, C. Stoeckl, T. C. Sangster, R. Olson, J. Kline, and J. Kilkenny, *Rev. Sci. Instrum.* **83**, 10D902 (2012).
- ²⁷D. Hicks, B. Spears, D. Braun, R. Olson, C. Sorce, P. Celliers, G. Collins, and O. Landen, *Phys. Plasmas* **17**, 102703 (2010).
- ²⁸The cryogenic DT ice layer of an ignition target is replaced with an equivalent mass of ablator material. The implosion dynamics are equivalent until deceleration and stagnation.
- ²⁹F. H. Séguin, J. A. Frenje, C. K. Li, D. G. Hicks, S. Kurebayashi, J. R. Rygg, B.-E. Schwartz, R. D. Petrasco, S. Roberts, J. M. Soures, D. D. Meyerhofer, T. C. Sangster, J. P. Knauer, C. Sorce, V. Y. Glebov, C. Stoeckl, T. W. Phillips, R. J. Leeper, K. Fletcher, and S. Padalino, *Rev. Sci. Instrum.* **74**, 975 (2003).
- ³⁰F. H. Séguin, N. Sinenian, M. Rosenberg, A. Zylstra, M. J.-E. Manuel, H. Sio, C. Waugh, H. G. Rinderknecht, M. G. Johnson, J. Frenje, C. K. Li, R. Petrasco, T. C. Sangster, and S. Roberts, *Rev. Sci. Instrum.* **83**, 10D908 (2012).
- ³¹A. B. Zylstra, J. A. Frenje, F. H. Séguin, M. J. Rosenberg, H. G. Rinderknecht, M. G. Johnson, D. T. Casey, N. Sinenian, M. J.-E. Manuel, C. J. Waugh, H. W. Sio, C. K. Li, R. D. Petrasco, S. Friedrich, K. Knittel, R. Bionta, M. McKernan, D. Callahan, G. W. Collins, E. Dewald, T. Döppner, M. J. Edwards, S. Glenzer, D. G. Hicks, O. L. Landen, R. London, A. Mackinnon, N. Meezan, R. R. Prasad, J. Ralph, M. Richardson, J. R. Rygg, S. Sepke, S. Weber, R. Zacharias, E. Moses, J. Kilkenny, A. Nikroo, T. C. Sangster, V. Glebov, C. Stoeckl, R. Olson, R. J. Leeper, J. Kline, G. Kyrala, and D. Wilson, *Rev. Sci. Instrum.* **83**, 10D901 (2012).
- ³²W. J. Hibbard, M. D. Landon, M. D. Vergino, F. D. Lee, and J. A. Chael, *Rev. Sci. Instrum.* **72**, 530 (2001).
- ³³J. Ziegler, J. Biersack, and U. Littmark, *The Stopping and Range of Ions in Matter* (Pergamon, New York, 1985).
- ³⁴Total correction is $\sim 1.5 - 2$ MeV. Uncertainty in the material thickness leads to an additional error of ± 50 to 75 keV in the total energy uncertainty.
- ³⁵The tent material is plastic with a thickness ≤ 100 nm, which the protons traverse nearly normally, so the areal density is $\ll 1 \text{ mg/cm}^2$. The hohlraum gas material has a density $\sim 1 \text{ mg/cm}^3$ with scale lengths of a few mm, so the areal density $< 1 \text{ mg/cm}^2$.
- ³⁶C. K. Li, F. H. Séguin, J. A. Frenje, R. D. Petrasco, P. A. Amendt, R. P. J. Town, O. L. Landen, J. R. Rygg, R. Betti, J. P. Knauer, D. D. Meyerhofer, J. M. Soures, C. A. Back, J. D. Kilkenny, and A. Nikroo, *Phys. Rev. Lett.* **102**, 205001 (2009).
- ³⁷A. B. Zylstra, C. K. Li, F. H. Séguin, M. J. Rosenberg, H. G. Rinderknecht, N. Sinenian, J. A. Frenje, R. D. Petrasco, N. Izumi, P. A. Amendt, O. L. Landen, and J. A. Koch, *Phys. Plasmas* **19**, 042707 (2012).
- ³⁸C. K. Li, A. B. Zylstra, J. A. Frenje, F. H. Séguin, N. Sinenian, R. D. Petrasco, P. A. Amendt, R. Bionta, S. Friedrich, G. W. Collins, E. Dewald, T. Döppner, S. H. Glenzer, D. G. Hicks, O. L. Landen, J. D. Kilkenny, A. J. Mackinnon, N. Meezan, J. Ralph, J. R. Rygg, J. Kline, and G. Kyrala, *New J. Phys.* **15**, 025040 (2013).
- ³⁹Such that the spherical harmonics are normalized, $\alpha = \sqrt{\frac{2\ell+1}{4\pi}} \frac{(\ell-m)!}{(\ell+m)!}$.
- ⁴⁰For the low modes considered, the variations are much larger than the detector solid angle ($\sim 1^\circ$ subtended) so using a local value of $R_{cm}(\theta, \phi)$ and thus $\rho R(\theta, \phi)$ is a good approximation.

- ⁴¹J. Kilkenny *et al.*, "Understanding the stagnation and burn of implosions on NIF," EPJ Conf. Ser. (submitted).
- ⁴²B. K. Spears, M. J. Edwards, S. Hatchett, J. Kilkenny, J. Knauer, A. Kritchler, J. Lindl, D. Munro, P. Patel, H. F. Robey, and R. P. J. Town, *Phys. Plasmas* **21**, 042702 (2014).
- ⁴³By fielding additional WRFs in key locations around the implosion the in-flight shape could be further constrained, for example at $\theta = 45^\circ$ to measure $\ell = 4$ modes; near the south pole at $\theta \sim 180^\circ$ to measure $\ell = 1$, and at multiple locations around the equator to constrain m modes.
- ⁴⁴D. K. Bradley, P. M. Bell, J. D. Kilkenny, R. Hanks, O. Landen, P. A. Jaanimagi, P. W. McKenty, and C. P. Verdon, *Rev. Sci. Instrum.* **63**, 4813 (1992).
- ⁴⁵M. S. Plessset, *J. Appl. Phys.* **25**, 96 (1954).
- ⁴⁶P. Amendt, J. D. Colvin, J. D. Ramshaw, H. F. Robey, and O. L. Landen, *Phys. Plasmas* **10**, 820 (2003).
- ⁴⁷M. Marinak, G. Kerbel, N. Gentile, O. Jones, D. Munro, S. Pollaine, T. Dittrich, and S. Haan, *Phys. Plasmas* **8**, 2275 (2001).
- ⁴⁸R. H. H. Scott, D. S. Clark, D. K. Bradley, D. A. Callahan, M. J. Edwards, S. W. Haan, O. S. Jones, B. K. Spears, M. M. Marinak, R. P. J. Town, P. A. Norreys, and L. J. Suter, *Phys. Rev. Lett.* **110**, 075001 (2013).
- ⁴⁹A. Kritchler *et al.*, APS DPP Bulletin, NO4.00004, 2013.
- ⁵⁰J. Gu, Z. Dai, Z. Fan, S. Zou, W. Ye, W. Pei, and S. Zhu, *Phys. Plasmas* **21**, 012704 (2014).
- ⁵¹A. Kritchler *et al.*, *Phys. Plasmas* **21**, 042708 (2014).
- ⁵²N. Izumi *et al.*, APS DPP Bulletin, BO1.010, 2004.
- ⁵³D. L. Bleuel, C. B. Yeamans, L. A. Bernstein, R. M. Bionta, J. A. Caggiano, D. T. Casey, G. W. Cooper, O. B. Drury, J. A. Frenje, C. A. Hagmann, R. Hatarik, J. P. Knauer, M. G. Johnson, K. M. Knittel, R. J. Leeper, J. M. McNamey, M. Moran, C. L. Ruiz, and D. H. G. Schneider, *Rev. of Sci. Instrum.* **83**, 10D313 (2012).
- ⁵⁴C. B. Yeamans, D. L. Bleuel, and L. A. Bernstein, *Rev. Sci. Instrum.* **83**, 10D315 (2012).
- ⁵⁵J. Frenje, R. Bionta, E. Bond, J. Caggiano, D. Casey, C. Cerjan, J. Edwards, M. Eckart, D. Fittinghoff, S. Friedrich, V. Glebov, S. Glenzer, G. Grim, S. Haan, R. Hatarik, S. Hatchett, M. G. Johnson, O. Jones, J. Kilkenny, J. Knauer, O. Landen, R. Leeper, S. L. Pape, R. Lerche, C. Li, A. Mackinnon, J. McNamey, F. Merrill, M. Moran, D. Munro, T. Murphy, R. Petrasso, R. Rygg, T. Sangster, F. Sguin, S. Sepke, B. Spears, P. Springer, C. Stoeckl, and D. Wilson, *Nucl. Fusion* **53**, 043014 (2013).
- ⁵⁶M. J. Edwards, P. K. Patel, J. D. Lindl, L. J. Atherton, S. H. Glenzer, S. W. Haan, J. D. Kilkenny, O. L. Landen, E. I. Moses, A. Nikroo, R. Petrasso, T. C. Sangster, P. T. Springer, S. Batha, R. Benedetti, L. Bernstein, R. Betti, D. L. Bleuel, T. R. Boehly, D. K. Bradley, J. A. Caggiano, D. A. Callahan, P. M. Celliers, C. J. Cerjan, K. C. Chen, D. S. Clark, G. W. Collins, E. L. Dewald, L. Divol, S. Dixit, T. Doeppner, D. H. Edgell, J. E. Fair, M. Farrell, R. J. Fortner, J. Frenje, M. G. Gatu Johnson, E. Giraldez, V. Y. Glebov, G. Grim, B. A. Hammel, A. V. Hamza, D. R. Harding, S. P. Hatchett, N. Hein, H. W. Herrmann, D. Hicks, D. E. Hinkel, M. Hoppe, W. W. Hsing, N. Izumi, B. Jacoby, O. S. Jones, D. Kalantar, R. Kauffman, J. L. Kline, J. P. Knauer, J. A. Koch, B. J. Kozioziemski, G. Kyrala, K. N. LaFortune, S. L. Pape, R. J. Leeper, R. Lerche, T. Ma, B. J. MacGowan, A. J. MacKinnon, A. Macphee, E. R. Mapoles, M. M. Marinak, M. Mauldin, P. W. McKenty, M. Meezan, P. A. Michel, J. Milovich, J. D. Moody, M. Moran, D. H. Munro, C. L. Olson, K. Opachich, A. E. Pak, T. Parham, H.-S. Park, J. E. Ralph, S. P. Regan, B. Remington, H. Rinderknecht, H. F. Robey, M. Rosen, S. Ross, J. D. Salmonson, J. Sater, D. H. Schneider, F. H. Sguin, S. M. Sepke, D. A. Shaughnessy, V. A. Smalyuk, B. K. Spears, C. Stoeckl, W. Stoeffl, L. Suter, C. A. Thomas, R. Tommasini, R. P. Town, S. V. Weber, P. J. Wegner, K. Widman, M. Wilke, D. C. Wilson, C. B. Yeamans, and A. Zylstra, *Phys. Plasmas* **20**, 070501 (2013).
- ⁵⁷L. Ballabio, J. Källne, and G. Gorini, *Nucl. Fusion* **38**, 1723 (1998).
- ⁵⁸H.-S. Bosch and G. Hale, *Nucl. Fusion* **32**, 611 (1992).
- ⁵⁹M. Rosenberg *et al.*, "A direct-drive exploding-pusher implosion for development of a monoenergetic proton, alpha, and triton backlighting platform at the National Ignition Facility," *Rev. Sci. Instrum.* (submitted).
- ⁶⁰M. Gatu Johnson, D. T. Casey, J. A. Frenje, C.-K. Li, F. H. Sguin, R. D. Petrasso, R. Ashabranner, R. Bionta, S. LePape, M. McKernan, A. Mackinnon, J. D. Kilkenny, J. Knauer, and T. C. Sangster, *Phys. Plasmas* **20**, 042707 (2013).